nature communications

Article

https://doi.org/10.1038/s41467-025-61783-1

Photomediated ion dynamics enables multi-modal learning, memory and sensing in ultralow-voltage organic electrochemical device

Received: 11 December 2024

Accepted: 1 July 2025

Published online: 28 July 2025

Check for updates

Guocai Liu[1,2,4], Wei Wen[1,2,4], Cong Shan[2], Haojie Huang[1,2], Yao Zhao[2,3], Yangshuang Bian[1,2], Yunlong Guo[1,2] ✉, Hui Huang[2] ✉ & Yunqi Liu[1,2] ✉

Ion signaling enables biological systems to implement learning, memory and sensing tasks in an energy-efficient manner. Organic electrochemical transistors are promising building blocks for mimicking ion-driven processes in the organism due to the iontronic coupling. However, the ion kinetics of diffusion back to the electrolyte poses a challenge in achieving non-volatility at ultralow gate voltages (V_G) required to mimic human learning and memory capabilities. Here we report a non-volatile heterojunction organic electrochemical device (nHOED) driven by photomediated ion trap and release dynamics. Due to the efficient separation of photogenerated charges within the heterojunction, the holes can be tightly trapped by anions at the photoactive layer−channel interface. This enables the device to realize multibit memory (over 100 distinct memory states) over a broad wavelength spectrum of 365–660 nm. Consequently, the nHOED can effectively replicate the learning, memory and sensing capabilities of the human neural system. In addition, the protocol avoids the injection of trap-function anions into the channel, facilitating the device to achieve non-volatility in the absence of V_G. Moreover, by employing a vertical traverse architecture that offers the advantage of a short channel, the operating voltage of the nHOED has been reduced to 0.1 V.

The human brain performs the sensing, learning, and memory tasks via high-parallel neural networks, which enable to us interact with the world in a fault-tolerant and energy-efficient way[1]. The development of neuromorphic devices that emulate brain function could, thus, provide more efficient scheme, especially in applications that are subject to low power and multitask. To create such a platform that fuses sensing, learning and memory is, however, challenging, due to the complex dynamics of ion channel and the fire model of biological neurons. To date, diverse building elements have been developed and widely adopted for use in neuromorphic electronics, mainly based on solid-state resistive devices, including two-terminal memristors[2,3], traditional organic transistors[4,5], and silicon-based complementary metal-oxide semiconductor circuits[6]. Nevertheless, neural devices made from these technologies are enabled by electronic charge transport, which is fundamentally different from the ion-based modulation mechanisms in biological systems, remaining limited potential in bio-integration, sensing, and response feedback[7–9].

[1]Beijing National Laboratory for Molecular Sciences, Key Laboratory of Organic Solids, Institute of Chemistry, Chinese Academy of Sciences Beijing, Beijing 100190, P. R. China. [2]University of Chinese Academy of Sciences, Beijing 101408, P. R. China. [3]Beijing National Laboratory for Molecular Sciences, Huairou Research Center, Institute of Chemistry, Chinese Academy of Sciences Beijing, Beijing 100190, P. R. China. [4]These authors contributed equally: Guocai Liu, Wei Wen. ✉e-mail: guoyunlong@iccas.ac.cn; huihuang@ucas.ac.cn; liuyq@iccas.ac.cn

Ions, as biosignal carriers, play a key role in energy-efficient information processing. The fundamental properties of biological entities set the requirements of the electronic counterpart. How to fully exploit ions is essential for the sustainable development of neuromorphic engineering and could bridge the gap between the biotic and the abiotic[10]. In this case, biocompatible fluidic memristors have been developed using interfacial nanochannel[11], polyelectrolyte-confined channel[12], 2D nanochannels[13], and highly asymmetric channels[14]. By tuning the channel conductance, data storage and processing abilities have been achieved. Despite these efforts, faithfully mimicking brain function is still a long-standing challenge, mainly because of the limited ability of the devices to sense and amplify electrophysiological signals. Organic electrochemical transistors (OECT) have emerged as crucial building blocks for neuromorphic devices and its core component, i.e., carriers transport channel, is in contact with physiologically relevant electrolytes. The unique iontronic coupling characteristic confers them a favorable ability to function as low-voltage biosensors[15,16] and transducer amplifiers[17,18]. However, the existing OECTs are restricted to volatility due to the diffusion of ion back to the electrolyte after the gate voltage (V_G) withdrawn. This presents a challenge in incorporating learning and memory behaviors in artificial neural systems, as it needs the ion kinetics contradictory with volatile behavior[7]. Several promising approaches have been employed to render organic electrochemical transistors capable of non-volatility by either decoupling the write and read operations using a "gate" electrode[19], or introducing a conductive bridge memory at the gate terminal[20], but this inevitably increases connection complexity. Recently, non-volatile OECTs without complicated electrical interconnections have been constructed by applying a large V_G[1,21] or V_G-assisted photo modulation[7]. Nevertheless, both require a high V_G to inject ions into the active channel layer to induce electrochemical doping. The energy efficiency and the memory capability are required to be further improved. Consequently, implementing non-volatile conductance modulation for multi-modal sensing, learning and memory on an ultralow operating-voltage OECT remains a significant challenge.

In this study, we constructed an ultralow-voltage non-volatile heterojunction organic electrochemical device (nHOED). A working mechanism of Photomediated ion trap and release dynamics (pITR) is developed. The channel holes are trapped by anions at the chlorophyll–poly(3-hexylthiophene) (P3HT) interface, thus avoiding the process of trap-function ions injection into the channel. The efficient separation of photogenerated charges within the heterojunction facilitates the robust trapping of holes, imparting long-term memory capability to the nHOED. This process parallels signaling processes observed in biological systems. Incorporating a vertical structure transistor characterized by short channel length, the operating voltage of the device is successfully reduced to 0.1 V and the memory could be realized at V_G of 0 V. Utilizing the advantages of non-volatility and ultralow operating voltage, biocompatible nHOED integrating learning, memory and sensing capabilities are demonstrated.

Results

Design of the bio-inspired nHOED

Hundreds of millions of neurons in the brain serve as the fundamental elements for signaling neural activity (Fig. 1a). Under external stimulus, ions including sodium and potassium are transported through ion channels to perform information processing and storage, giving rise to intelligent behaviors[22]. The operating mechanism of the nHOED in this work resembles that of the biological nerve. The device adopts a vertical structure to reduce the operating voltage, which benefits from a very small channel length (~36 nm), as shown in Fig. 1b and Supplementary Fig. 2. The natural chlorophyll/P3HT heterojunction is employed with the aim of enhancing the biocompatibility and facilitating charge separation to increase the carrier concentration. The natural chlorophyll serves as photoactive layer and P3HT is conducting

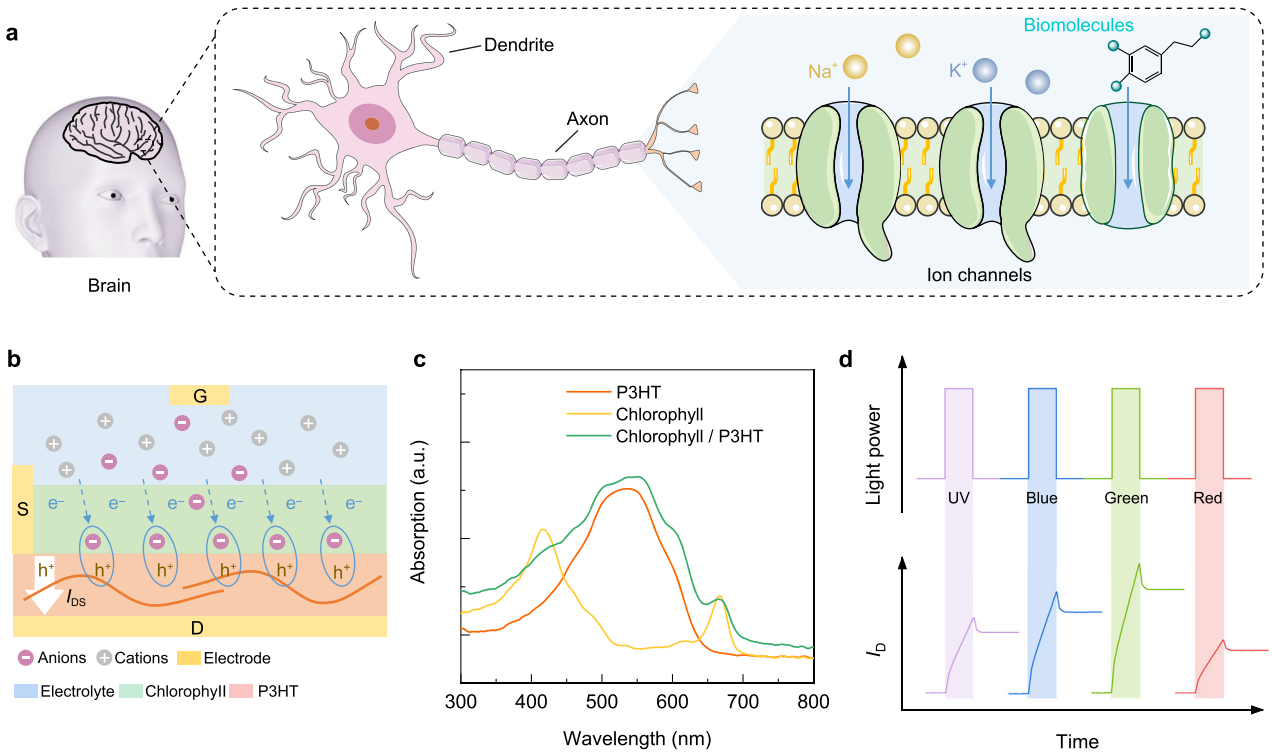

Fig. 1 | Conceptual scheme of the nHOED. a, Schematic illustration of a biological neuron. The basic biological events are generated by rapid transmembrane ion exchange through ion channels, and they propagate along the axon. **b**, Device architecture of a vertical structure nHOED with ions migration and accumulation. **c**, UV-vis spectra of P3HT, chlorophyll, and chlorophyll/P3HT films. **d**, Ion-mediated memory behavior of nHOED under a broadband light illumination.

channel, where heterojunction exhibit lower transmittance (Supplementary Fig. 3). When excited by illumination, the heterojunction generates electron-hole pairs and the separated holes are transported as majority carriers. Under the influence of electrostatic coupling, anions in the electrolyte move towards the chlorophyll–P3HT interface to compensate for the holes, forming an electric double layer (EDL) at the interface. Meanwhile, the anions act as traps to capture holes, resulting in the non-volatile behavior. The transfer characteristics and the real-time currents of the nHOED measured under 520 nm light illumination at various intensity and exposure time are shown in Supplementary Figs. 4 and 5. Both a noticeable current increase and non-volatility could be observed. Figure 1c and Supplementary Fig. 6 show the UV-vis absorption spectra of P3HT film, chlorophyll film, and chlorophyll/P3HT film. Noted that chlorophyll/P3HT film absorbs light mainly in the UV-vis region. Based on the light-absorbing properties of the device, we investigated its non-volatile memory features over a wide range in the UV-visible region in this work (Fig. 1d).

Ion-modulated non-volatile behavior

To investigate the non-volatile mechanism of nHOED, the program-erase cycle test of the devices (Fig. 2a and Supplementary Fig. 7) was conducted. The cycle is divided into four distinct states, i.e., initial, programming, memory, and erasing states. In the initial state, the anions and cations in the electrolyte are randomly distributed, resulting in an unobvious I_{DS}. During the light-induced programming process, the electron-hole pairs are generated in the heterojunction and subsequent separation, wherein holes are transported from chlorophyll to P3HT (Supplementary Fig. 8), thereby producing a substantial I_{DS} under the applied V_D. Meanwhile, the transportation of holes induces a positive charge on the channel side, which attracts anions drifting towards and accumulate at the chlorophyll–P3HT interface to balance the charge by compensating for the holes. In this process, anions act as traps for binding with holes, leading to the formation of an EDL. Despite a reduction in the number of holes and a subsequent drop in current after the light is withdrawn, the presence of the trapped holes by anions enables the conductance of the channel to maintain at a high level. The efficient charge separation within the heterojunction facilitates the firm trapping of holes[7]. This endows the nHOED with a long-term non-volatile memory. To release the trapped holes, it is necessary to apply an electric field that serves to break electrostatic balance between the anions and the trapped holes. Here a positive gate voltage is applied at the gate terminal. It facilitates the diffusion of anions back into the electrolyte, thereby releasing the trapped holes. Consequently, the concentration of holes within the channel reduced, resulting in a decrease in channel conductance.

To verify the hypothesis, we subjected the nHOED to five consecutive light pulses while varying the V_G, as illustrated in Fig. 2b. It can be noted that the device exhibits phototransistor characteristics, whereby the current drops to the baseline instantaneously upon the cessation of light exposure. Conversely, as the V_G decreases to 0 V, the device performs non-volatile memory, wherein the current decays slowly and stabilizes at a relatively elevated level after light withdrawal. Meanwhile, the retention current, i.e., steady state current increases gradually with increasing number of light pulses. Upon the application of a negative V_G, the current variation between the retention and peak value following the removal of light diminishes until it aligns with the peak current observed at a V_G of −0.5 V. This indicates a progressive reinforcement in non-volatile memory, ultimately achieving an optimal memory state. The memory level ($L_M = (I_{retention} - I_{initial})$, where $I_{retention}$ is the retention current after being programmed by each light pulse, $I_{initial}$ is the initial current before being programmed) of the device in five memory states (states after being programmed) at different V_G is shown in Fig. 2c. It can be obtained that the memory level of the device improves gradually with pulse number increasing, indicating the continuous conductance tunability of the nHOED by light-induced ion-trapped holes. To demonstrate the memory difference at various V_G, the memory capability ($C_M = (I_{retention} - I_{dark}) / (I_{peak} - I_{dark})$*100%, where $I_{retention}$, I_{dark} are the retention current and dark current before/after being programmed by each light pulse, I_{peak} is the corresponding peak current) of the device is illustrated in Fig. 2d. When the V_G is in the positive region, the value of C_M is close to 0%; however, as the V_G varies from 0 V to negative region, C_M increases significantly and reaches 100% at V_G of −0.5 V. It means that negative V_G is beneficial for enhancing memory capacity. This is due to that negative V_G prevents the counterions from compensating for the anions[23], inducing a stable anion layer at the chlorophyll–P3HT interface for trapping holes. In contrast, positive V_G retracts the anions, and is detrimental to the trapping. It is worth noting that the device displays memory characteristics at V_G of 0 V, where the minimum operating voltage of the nHOED, i.e., the read voltage V_D is −0.1 V, much lower than that observed in previously reported transistor memories (Supplementary Table 1). This is attributed to the fact that the hole-trapping anions do not have to be injected into the channel, but simply accumulate at the chlorophyll–P3HT interface for trapping holes, thus significantly reducing the operating voltage of the memory. The phenomenon can be validated by the spectroelectrochemistry of chlorophyll/P3HT film and P3HT film before and after light exposure (Fig. 2f, g). After a 5 s light exposure, a decrease in the visible region and an increase at the near-infrared region could be observed in the spectra of chlorophyll/P3HT film but no changes of P3HT film. It can also be validated by the TOF-SIMS depth profiling (Supplementary Fig. 9). The $TFSI^-$ signal only occurs at the top layer of the heterojunction. These results suggest that only the chlorophyll film is doped during the process of light programming, which probably because the built-in electric field in the chlorophyll prevents the trap-function anions from doping the channel. Moreover, doping ions are anions not cations and the doped film can return to the original state by electrical erasing (Supplementary Figs. 10 and 11). As illustrated in Supplementary Fig. 12, the P3HT alone film could maintain its initial state during the program-erase operation and V_G could make anions electrochemical doping the P3HT. To further demonstrate the trapping mechanism, additional characterization is necessary. Figure 2h shows the performance difference of the devices with/without chlorophyll. Relative to nHOED, the devices without chlorophyll lack memory capability and have a lower photocurrent. This is due to the inefficient charge separation in P3HT (Fig. 2i), where the holes are challenging to be readily trapped by anions, highlighting the significant role of the chlorophyll/P3HT heterojunction in the ion trapping process. Meanwhile, the fluorescence lifetime of P3HT (Fig. 2j) is prolonged after adding chlorophyll is due to the transfer of photogenerated electrons to chlorophyll, which increases the relaxation time of excitons of P3HT in the excited state. In terms of chlorophyll, the decay becomes faster after adding P3HT because the transfer of photogenerated holes to P3HT introduces a non-radiative transition pathway, resulting in a reduced lifetime. The photoluminescence (PL) spectra reveals a significant charge transfer process from chlorophyll to P3HT[24].

The absorption spectra presented in Fig. 1c demonstrates that the chlorophyll/P3HT heterojunction film exhibits varying capacities for light absorption within the UV-vis region. Accordingly, we hypothesize that the nHOED displays disparate memory behaviors within this spectral region, which is related to the separation efficiency (E_S) of electron-hole pairs (Fig. 3a). Figure 3b illustrates the theoretically studied t-index of the heterojunction when excited by light of various wavelengths, with the order being $t_{green} > t_{blue} > t_{UV} > t_{red}$. The t-index quantifies the extent of separation of photogenerated electron-hole pairs (see Methods). A positive t-index value refers to a greater degree of separation, resulting in a higher E_S. The research indicates that a high degree of separation of the photogenerated hole-electron pairs is favorable for ion trapping, thereby enhancing memory level[25]. The corresponding current response, as depicted in Fig. 3c, varies when

https://doi.org/10.1038/s41467-025-61783-1

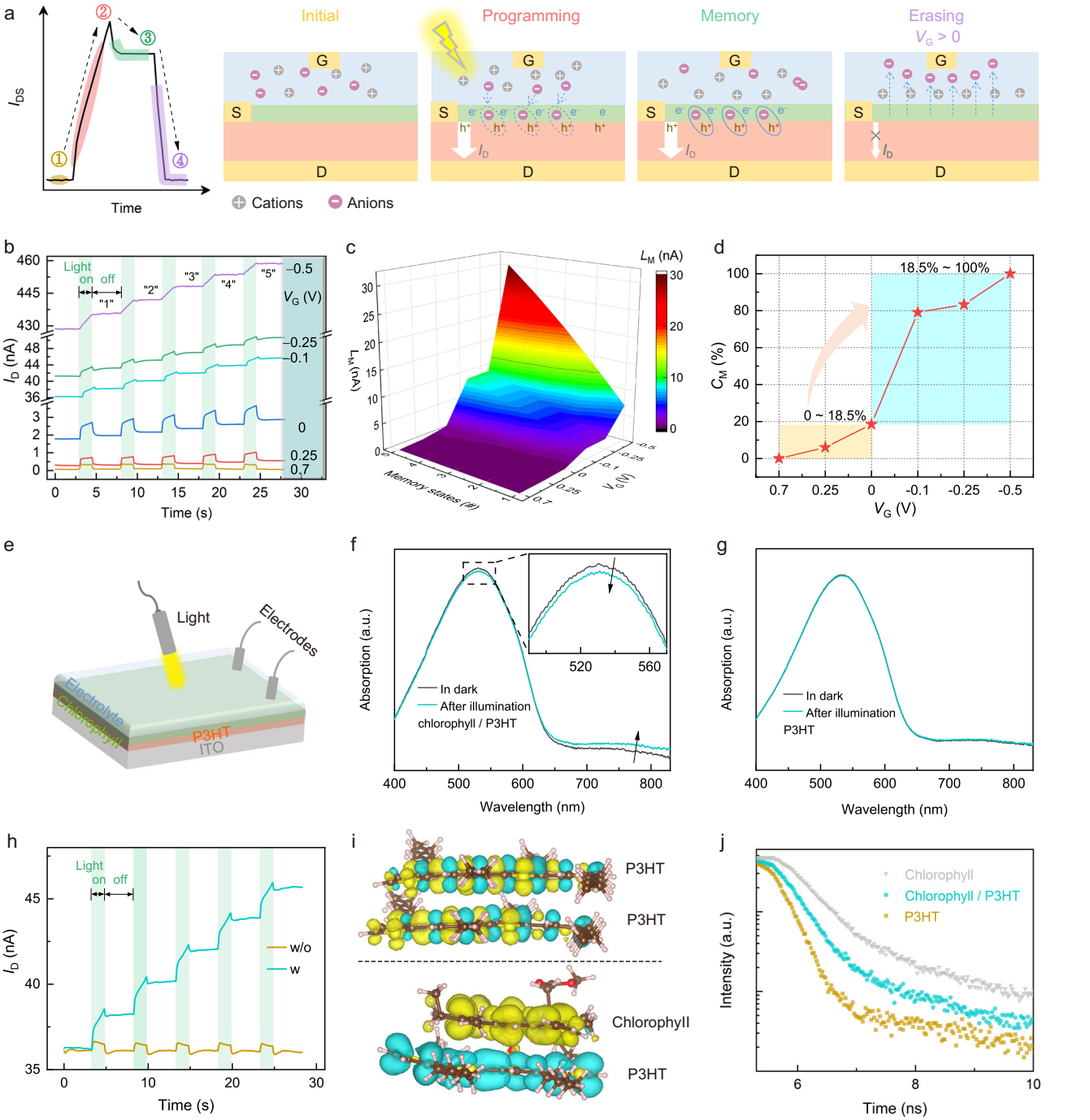

Fig. 2 | Mechanism of ion-mediated non-volatility. a, Schematic illustrations of an ion-modulated program-erase process. **b,** V_G-dependent non-volatility under five 520 nm light pulses (0.1 mW cm^{-2}, 1.5 s). **c,d**, Effect of V_G on memory level (L_M) (**c**) and memory capability (C_M) (**d**) in five memory states. V_D is fixed at −0.1 V. **e**, Schematic illustration of spectroscopic measurements. **f,g**, Spectroelectrochemistry of chlorophyll/P3HT film (**f**) and P3HT film (**g**) before and after light illumination (520 nm, 0.1 mW cm^{-2} for 5 s) at V_G = −0.5 V. **h**, The time-dependent output currents of the devices with/without chlorophyll are measured at V_G, V_D = −0.1 V under five sequential light pulses (520 nm, 0.1 mW cm^{-2} for 1.5 s). **i**, Theoretical studies on the charge separation of active layer with/without chlorophyll. The colors blue and orange represent holes and electrons, respectively. **j**, Time-resolved PL spectra of chlorophyll, P3HT and chlorophyll/P3HT obtained at 650 nm with excitation wavelength of 400 nm.

subjected to five consecutive light pulses at wavelengths of 365 nm (UV), 450 nm (blue), 520 nm (green), and 660 nm (red), respectively. The results confirm the presence of memory behaviors in this broadband region, albeit with differing levels. Moreover, the device displays the most pronounced current variation under green light, followed by blue light, with UV and red light inducing comparatively minor changes, which is consistent with the theoretical calculations. In addition, the current variation of nHOED programmed by multiple consecutive light pulses, as illustrated in Fig. 3d and Supplementary Fig. 13, demonstrates the multibit memory capability under a broadband spectrum, encompassing over 100 distinct memory states. Meanwhile, the current maintained well at different spikes (Supplementary Fig. 14). This is achieved through a stepwise current change, which is tuned by an increased concentration of ion-trapped holes. Figure 3e records the

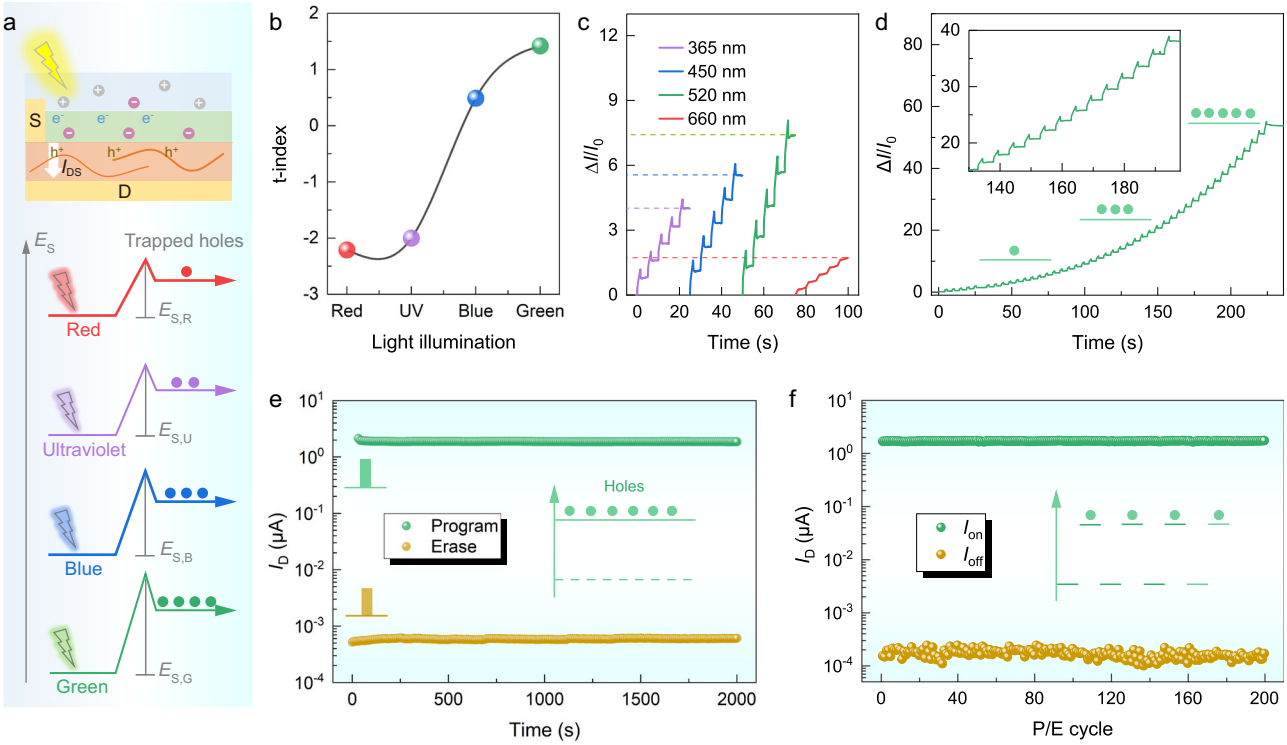

Fig. 3 | Multibit memory behaviors under the broadband lighting. a, Schematic illustrations of the changes in separation efficiency of electron-hole pairs under different light conditions, where $E_{S,R}$, $E_{S,U}$, $E_{S,B}$, $E_{S,G}$ are separation efficiency of electron-hole pairs excited by light of red, UV, blue, and green, respectively. The purpose is to show visually the effect of light wavelength on the optoelectronic properties. **b**, Theoretical calculated t-index of the nHOED excited by varying light conditions, which represents the extent of charge separation. **c**, Representative five memory states of the device stimulated by broadband light within the wavelength range of UV-vis region (0.1 mW cm^{-2} for 1.5 s, intervals 3.5 s, V_D and V_G of −0.1 V). **d**, Multibit memory states programmed by sequential 520 nm light pulses (0.1 mW cm^{-2} for 1.5 s, intervals 3.5 s, V_D and V_G of −0.1 V). **e**, Retention performance of the nHOED after the light program (520 nm, 0.83 mW cm^{-2} for 30 s, V_D = −0.1 V and V_G = 0 V) and voltage erase (V_G of 1 V for 5 s, V_D = −0.1 V) operations, reading at V_D = −0.1 V and V_G = 0 V. **f**, Endurance test under 200-program/erase (P/E) cycles: programmed by 520 nm light pulse (0.83 mW cm^{-2} for 30 s, V_D = −0.1 V and V_G = 0 V), on-current reading for 20 s at V_D = −0.1 V and V_G = 0 V, erased by a V_G pulse (1 V for 5 s), off-current reading at V_D = −0.1 V and V_G = 0 V for 10 s.

retention characteristics of the nHOED memories. All current states are observed to maintain stability for a duration exceeding 2000 seconds, which is indicative of a stable non-volatile feature. Furthermore, operations of program-read-erase-read for 200 cycles were carried out, as shown in Fig. 3f and Supplementary Fig. 15. The memory device maintains a high on/off ratio of 10^3 without any decay, demonstrating the superior memory durability[26,27].

Visual recognition

Color serves as a visual stimulus making a significant impact on improving human cognition (Fig. 4a). It has been demonstrated that the use of colored multimedia materials facilitates learning and memory by enhancing cognitive engagement[28]. Acetylcholine (ACh) signaling in the cortex is well known to be involved in advanced cognitive functions, such as learning and memory (Fig. 4b). A decline in ACh levels has been linked to a reduction in cognitive function in individuals diagnosed with Alzheimer's disease[29]. The ability to reproduce the impact of color on ACh release, and consequently on visual memory, is crucial for neuromorphic devices[30]. To evaluate the potential of the visual recognition quantitatively, we have proposed an artificial photonic neuromorphic system with nHOED. A convolutional neural network was implemented and a 28 × 28-pixel image of handwritten digits of "8" from the Modified National Institute of Standards and Technology (MNIST) handwritten data set was employed for the purpose of learning. As illustrated in Fig. 4c, the network comprises 784 input neurons and 10 output neurons (ranging from 0 to 9), with complete connectivity through parallel synaptic weights. Ion migration of nHOED induced by light at different wavelengths parallels the process of ACh release from the cerebral cortex stimulated by different colored texts. The changes in the weights of nHOED, resulting from exposure to various colored light, can simulate the activity of ACh in the human brain in response to learning different colored texts. Specifically, light wavelengths of 450 nm, 520 nm, and 660 nm represent blue, green, and red light, respectively (a fixed light intensity of 0.1 mW/cm^{-2}). The accuracy of the nHOED on image recognition under the light stimulation of different wavelengths is shown in Fig. 4d. When the nHOED exposed to green light the highest accuracy of 0.963 was obtained, followed by that exposed to blue light, while red light yields the lowest accuracy of 0.933. These results suggest that green text facilitates the release of ACh in the cerebral cortex, thereby enhancing memory (Supplementary Text 1 and Supplementary Fig. 16)[31]. This phenomenon can be primarily attributed to the calming and comforting effects of green and blue colors, which activate a greater number of brain regions[32,33]. Figure 4e and Supplementary Fig. 17 present the confusion matrix for categorizing various handwritten digits. The highest probability value in each row of predicted output is highly consistent with the target output, effectively demonstrating their performance in object recognition. Above results suggest the nHOED has the potential for visual recognition and neuromorphic computing.

Stretchable ECG sensors

Stretchable electronics can intimately integrate with human bodies to provide continuous monitoring of physiological signals without constraining movement. But it is difficult to achieve stretchable nHOED, due to its vertically laminated architecture. To prevent mechanical strain from causing nHOED performance degradation, we implemented an island-bridge structure, as illustrated in Fig. 5a. The island is a

https://doi.org/10.1038/s41467-025-61783-1

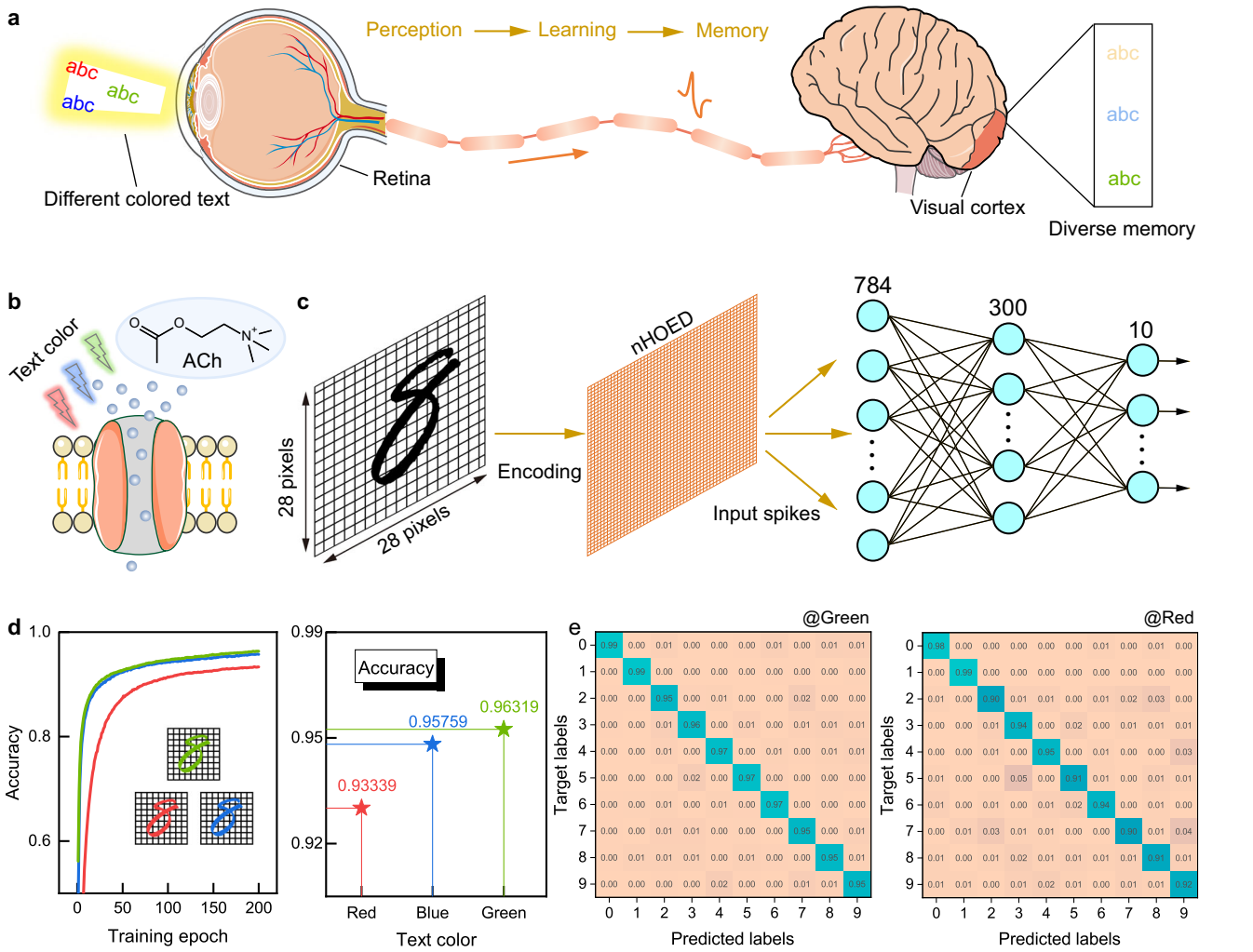

Fig. 4 | Color mediated learning and memory behaviors. a, Schematic illustration of the human visual system that text colors enable different memories. **b**, Schematic diagram of acetylcholine (Ach) secretion in organism during the learning process. **c**, A schematic representation of a text color recognition system designed to identify three distinct text colors. **d**, The recognition accuracy evolution with training epochs for 28 × 28-pixel handwritten digit image of RGB colors. **e**, Confusion matrix of training results at green and red light.

patterned regions of mechanical heterogeneity into the elastomer substrates, containing a rigid elastiff layer and a functional layer superimposed upon it. Under mechanical deformation, the hard elastiff layer can preserve its initial shape, which is favorable to maintain the electrical properties of the functional layer. To facilitate robust interfacial interactions, the rigid elastiff and the soft substrate materials are derived from the same family of polystyrene-block-poly(ethylene-ran-butylene)-block-polystyrene (SEBS) elastomers with 67 vol% and 12 vol% polystyrene, respectively. They exhibit comparable chemical compositions; however, differences in their modulus result in distinct mechanical properties[34]. Adopting Au as the source-drain electrode serves dual purposes: it aids in achieving energy level alignment to enhance charge transfer, and it contributes to maintaining a smooth contact surface between the active layer and the electrode within the vertical configuration. The bridge is composed of patterned serpentine-shaped silver nanowires that serve to interconnect the islands. With the advantage of high stretchability, it can be leveraged to maintain the conductivity of the electrodes during the stretching process. The preparation process for the stretchable nHOED featuring island-bridge structures is illustrated in Supplementary Fig. 18 and corresponding optical photographs of P3HT patterning, elastiff layer, and overall stretchable devices are shown in Supplementary Fig. 19. The obtained nHOED exhibit superior tensile characteristics in both stretching and poking situations (Fig. 5b and Supplementary Movie). As demonstrated by mechanical simulations, the application of a 100% local strain to the device integrated with the elastiff layer resulted in the island undergoing only a minor local strain referred to as the strain on the substrate (Fig. 5c and Supplementary Fig. 20), allowing the functional layers to maintain performance stability. When subjected to strain of 25% over 1000 repeated stretching-releasing cycles, the current under dark (I_{dark}) and light (I_{light}) conditions of the fabricated stretchable nHOED sustained relatively constant values. During the stretching from 0% to 100% strain, the I_{dark} and I_{light} only displayed minor changes at 100% (Fig. 5d and Supplementary Fig. 21). These results demonstrate the excellent mechanical stability of the device, attributable to the island's ability to sustain minimal deformation during the device's overall deformation and the constant conductivity of the electrode (Supplementary Figs. 22 and 23). The lower modulus of substrate facilitates greater strains during deformation and the higher modulus of elastiff layer yields comparatively smaller strains. Additionally, when stored in air under dark for 60 days, the performance of the nHOED displayed little degradation (Supplementary Fig. 24), due to the high environment stability of natural chlorophyll and P3HT. Stable electrical performance and low operating voltage are crucial in various applications that require reliable signal output, particularly in the presence of biosignal and mechanical deformation. To demonstrate the applicability of the

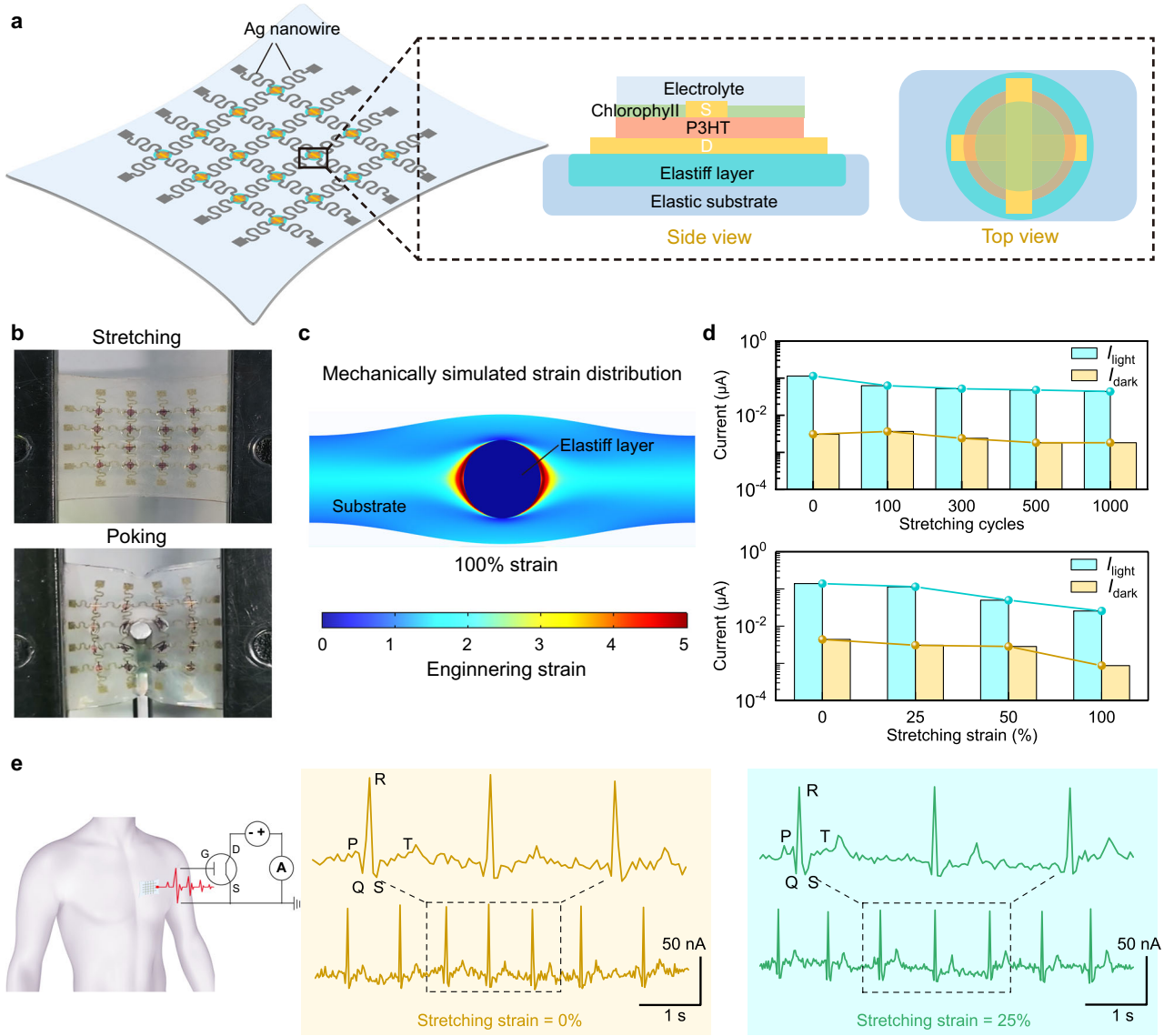

Fig. 5 | Design of island-bridge nHOED and its sensing behaviors. a, Device architecture of the stretchable vertical ion-gated transistor array involves SEBS elastic substrate, functional islands, and serpentine Ag nanowire interconnects. **b**, Optical microscope images of the device under stretching and poking deformations. **c**, Mechanical simulation showing the strain distribution of a transistor for stretching under 100% strain. **d**, I_{light} and I_{dark} under stretching strains from 0% to 100% and after multiple stretching-releasing cycles of up to 1000 times at 25% strain. **e**, Illustration of ECG recording and spontaneous heart activity measured on a human subject with the device under stretching strains of 0%, and 25%. Inset: the enlarged ECG signals under stretching strain of 0% and 25%, respectively.

low-voltage stretchable nHOED for skin-conformable sensing of physiological signals, the real-time recorded ECG signals are shown in Fig. 5e. When the ECG signal is applied between the gate and source electrodes of the nHOED, the resulting drain current serves as the recording signal without gate voltage[35]. The ECG recording shows all the expected waveforms (P, Q, R, S, and T waves). Remarkably, when the current nHOED is subjected to strain of 0% and subsequently 25%, comparable ECG recordings are achieved and exhibiting significant signal-to-noise ratio (SNR) of 35.3 dB and 32.9 dB, respectively. Thanks to its stable sensing properties, it is expected to develop into portable and wearable ECG sensors for early detecting signs of heart disease and continuous health monitoring.

Discussion

We developed an pITR strategy, wherein holes are trapped at the chlorophyll–P3HT interface, enabling nHOED with non-volatility. Negative V_G is beneficial for trapping holes with preventing the cations from compensating for the anions, which resulted in an enhanced memory capacity. By constructing a converse vertical structure with the advantage of short channels, the working voltage of the nHOED is reduced to 0.1 V and the non-volatility could be achieved at V_G of 0 V. In the wavelength range from 365 nm to 660 nm, the nHOED displays multibit memory (exceeding 100 distinct memory states), which is exploited to emulate the brain's ability to learn and memorize different colored text. Under green light, the nHOED displays the most significant memory level and exhibits the highest image recognition accuracy of 0.963. Finally, we designed an island-bridge structure that enables nHOED superior stretchability. Taking advantage of the low operation voltage of the nHOED, a stretchable ECG monitoring sensor was constructed and it exhibits excellent ECG signal stability even when subjected to a strain of 25%.

Methods

Materials

Poly(3-hexylthiophene) and chlorophyll were purchased from TCI. SEBS (H1221) with a volume fraction of poly(ethylene-co-butylene) of 88% and

rigid SEBS (H1043) with a volume fraction of poly(ethylene-co-butylene) of 33% were purchased from Asahi Kasei. SEBS H1043 was employed as the elastiff layer and SEBS H1221 was employed as the stretchable substrate in the stretchable devices. 1,6-bis(trichlorosilyl)hexane and electrolyte 1-ethyl-3-methylimidazolium bis(trifluoromethylsulfonyl)imide (EMIM:TFSI) were purchased from Sigma–Aldrich. All the processing solvents, such as 1, 2-dichlorobenzene and n-hexane were purchased from commercial sources and used as received.

Fabrication of nHOED

Glass substrates were cleaned with detergent first, and rinsed with deionized water, ethanol, and isopropanol, and finally dried by N_2. The bottom drain electrode (Au, 30 nm) with 90 μm width was thermally deposited on the substrate. The P3HT blended with the 1,6-bis(trichlorosilyl)hexane was spin-coated (3000 rpm, in 1, 2-dichlorobenzene, 10 mg mL^{-1}) and annealed at 140 °C for 3 h and the thickness of ~36 nm. The top electrode (Au, 30 nm) with 90 μm width was thermally deposited the sample. Chlorophyll solution (0.5 mg/mL in n-hexane) was spray-coated for 60 s and the solvent was evaporated naturally with the resultant thickness of ~7.2 nm. Electrolyte of EMIM:TFSI was dropped on the crossing point of the bottom and top electrodes, thus the channel was covered.

Fabrication of stretchable devices

Dextran (15 wt%) was dissolved in water and spin coated on the oxygen plasma-treated glass (100 W, 2 min) and subsequently annealed at 90 °C for 30 minutes. The preparation process of electrodes and semiconductor solutions is consistent with that previously described for use on rigid glass. By directional etching (50 W, 6 min) with a mask, the P3HT was removed everywhere except around the top contacts, thus the Au electrodes around the crossing point are exposed. Serpentine-shaped Ag nanowire electrodes were applied via spray coating to the Au of the exposure region, thereby forming a bridge structure that interconnects the island components. SEBS (H1043) solution was dropped on the connection region of the Au and Ag nanowire and annealed at 40 °C to form elastiff layer. Subsequently, SEBS (H1221) solution (in n-hexane, 100 mg/ml) was dropped on the sample to form a stretchable substrate. After that, the whole device was soaked in water to dissolve the dextran and transfer all the components onto the substrate. Chlorophyll solution was spray-coated and solvent was evaporated naturally. The electrolyte of EMIM:TFSI was deposited at the intersection of the bottom and top electrodes, covering the channel.

Computational methods

The charges separate at the interface, and to clearly demonstrate the charge separation properties we performed computational calculation using two layers of molecules. The heterojunction molecule is stacked as chlorophyll/P3HT and the chlorophyll free, i.e. pure P3HT, is stacked as P3HT/P3HT. All calculations were carried out by adopting Gaussian 09 (E.01) package. Structural optimizations were performed at the B3LYP/6-31 G* level with dispersion correction of Grimme's DFT-D3(BJ). The electron excitation calculations were realized by time-dependent DFT (TD-DFT) using PBE0 exchange-correlation functional in conjunction with 6-311 G* basis set in the gas phase. The electron density difference between the excited state and ground state, along with the t-index that measures the degree of separation between holes and electrons, is determined using hole-electron analysis with the support of Multiwfn 3.8(dev)[36]. t-index is designed to measure separation degree of hole and electron in charge transfer (CT) direction: t-index = D-index − H_{CT}, where the total magnitude of CT length is referred to as D-index, H_{CT} measures average degree of spatial extension of hole and electron distribution in CT direction. If t-index<0, it implies that hole and electron is not substantially separated due to CT. Clear separation of hole and electron distributions must correspond to evidently positive t-index. The isosurface maps of charge density difference was visualized by VESTA based on the files exported by Multiwfn.

Device characterizations

Optical microscopy images were captured with an Olympus BX51 microscope. Electrical performances of nHOED was characterized by semiconductor parameter analyzer Keithley 4200 SCS and Keysight B2912A at room temperature. Red, green, blue and UV light emitting diodes (LEDs) were utilized to offer light source with fixed wavelength. The light intensity of the LEDs was detected by a Si photodiode, and the electrical input power of the LEDs was adjusted with a DC power supply (MESTEK DP305) to change the illumination intensities. Rigol DG 5000 were conducted to provide a square pulse signal to generate pulsed light. To measure the OECT at different strain levels, the devices were held under a strain and the EMIM-TFSI was dropped directly onto the channel region. To prevent the ionic liquid from moving, the strain was achieved by slowly adjusting the stage. For the cycle test, the ionic liquid was blown off during the repeated stretch-release cycles and was dropped onto the channel area until the next cycle stage. TOF-SIMS-M6 (ION-TOF GmbH, Germany) analysis with Bi_3^+ (30 keV) as the primary ion source was used to determine the doping profile, where negative secondary ions from an area of 100 × 100 $μm^2$ were detected. Sputter etching was performed over an area of 300 × 300 $μm^2$ using an Cs^+ ion beam with an acceleration voltage of 1 kV. The currents of the primary ion beam and Ar gas cluster ion beam were 0.15 pA and 100 nA, respectively. An electron flood gun was applied for charge neutralization.

ECG measurement

In the context of ECG measurement, the drain current acts as output signal. Two electrodes were attached to the skin near the heart and connected to the source and gate terminal, respectively. The SNR of ECG signals are calculated using the equation: $SNR(dB)=20lg(A_{signal}/A_{noise})$, where A_{signal} is amplitude of signal during a period of activity and A_{noise} is the standard deviation of the noise. The experiments of in vitro ECG recording were performed in compliance with the protocol approved by the Science and Technology Ethics Committee of the University of Chinese Academy of Sciences (No: UCASSTEC25-017). The participant (the first author, G.L.) followed informed consent and appropriate assessment of the risks involved.

Reporting summary

Further information on research design is available in the Nature Portfolio Reporting Summary linked to this article.

Data availability

All data needed to evaluate the conclusions in the paper are present in the paper and/or the Supplementary Information. Source data are provided with this paper. Additional data related to this paper may be requested from the authors. Source data are provided with this paper.

References

1. Ji, X. et al. Mimicking associative learning using an ion-trapping non-volatile synaptic organic electrochemical transistor. *Nat. Commun.* **12**, 2480 (2021).
2. Kim, G. et al. Mott neurons with dual thermal dynamics for spatio-temporal computing. *Nature Materials* **23**, 1237–1244 (2024).
3. Liu, K. et al. An optoelectronic synapse based on α-In_2Se_3 with controllable temporal dynamics for multimode and multiscale reservoir computing. *Nature Electronics* **5**, 761–773 (2022).
4. Yan, X. et al. Moiré synaptic transistor with room-temperature neuromorphic functionality. *Nature* **624**, 551–556 (2023).
5. Zhu, X. et al. High-contrast bidirectional optoelectronic synapses based on 2D molecular crystal heterojunctions for motion detection. *Advanced Materials* **35**, 2301468 (2023).

6. Mahowald, M. & Douglas, R. A silicon neuron. *Nature* **354**, 515–518 (1991).
7. Chen, K. et al. Organic optoelectronic synapse based on photon-modulated electrochemical doping. *Nature Photonics* **17**, 629–637 (2023).
8. Harikesh, P. C. et al. Organic electrochemical neurons and synapses with ion mediated spiking. *Nat. Commun.* **13**, 901 (2022).
9. Harikesh, P. C. et al. Ion-tunable antiambipolarity in mixed ion-electron conducting polymers enables biorealistic organic electrochemical neurons. *Nature Materials* **22**, 242–248 (2023).
10. Tybrandt, K., Larsson, K. C., Richter-Dahlfors, A. & Berggren, M. Ion bipolar junction transistors. *Proc Natl Acad Sci USA* **107**, 9929–9932 (2010).
11. Zhang, P. et al. Nanochannel-based transport in an interfacial memristor can emulate the analog weight modulation of synapses. *Nano Lett* **19**, 4279–4286 (2019).
12. Xiong, T. et al. Neuromorphic functions with a polyelectrolyte-confined fluidic memristor. *Science* **379**, 156–161 (2023).
13. Robin, P. et al. Long-term memory and synapse-like dynamics in two-dimensional nanofluidic channels. *Science* **379**, 161–167 (2023).
14. Emmerich, T. et al. Nanofluidic logic with mechano-ionic memristive switches. *Nature Electronics* **7**, 271–278 (2024).
15. Nawaz, A. et al. Organic Electrochemical transistors for in vivo bioelectronics. *Advanced Materials* **33**, 2101874 (2021).
16. Liu, G. et al. Bionic tactile-gustatory receptor for object identification based on all-polymer electrochemical transistor. *Advanced Materials* **35**, 2300242 (2023).
17. Huang, W. et al. Vertical organic electrochemical transistors for complementary circuits. *Nature* **613**, 496–502 (2023).
18. Liu, G., Guo, Y. & Liu, Y. Design of ion-gated transistor materials at the molecular level. *Matter* **7**, 430–455 (2024).
19. van de Burgt, Y. et al. A non-volatile organic electrochemical device as a low-voltage artificial synapse for neuromorphic computing. *Nature Materials* **16**, 414–418 (2017).
20. Fuller, E. J. et al. Parallel programming of an ionic floating-gate memory array for scalable neuromorphic computing. *Science* **364**, 570–574 (2019).
21. Wang, S. et al. An organic electrochemical transistor for multimodal sensing, memory and processing. *Nature Electronics* **6**, 281–291 (2023).
22. Lee, H.-R., Kim, C.-C. & Sun, J.-Y. Stretchable ionics - a promising candidate for upcoming wearable devices. *Advanced Materials* **30**, 1704403 (2018).
23. Kweon, H. et al. Ion trap and release dynamics enables nonintrusive tactile augmentation in monolithic sensory neuron. *Science Advances* **9**, eadi3827 (2023).
24. Yang, B. et al. Bioinspired multifunctional organic transistors based on natural chlorophyll/organic semiconductors. *Advanced Materials* **32**, 2001227 (2020).
25. Lai, H. et al. Fast, multi-bit, and vis-infrared broadband nonvolatile optoelectronic memory with MoS_2/2D-perovskite van der waals heterojunction. *Advanced Materials* **35**, 2208664 (2023).
26. Chen, C.-H. et al. Novel photoinduced recovery of OFET memories based on ambipolar polymer electret for photorecorder application. *Advanced Functional Materials* **29**, 1902991 (2019).
27. Hsu, C.-W. et al. Spider silk/hemin biobased electrets for organic phototransistor memory: a comprehensive study on solution process engineering. *Advanced Functional Materials* **34**, 2314907 (2024).
28. Chai, M. T. et al. Exploring EEG effective connectivity network in estimating influence of color on emotion and memory. *Front. Neuroinform.* **13**, 66 (2019).
29. Qi, X.-L. et al. Nucleus basalis stimulation enhances working memory by stabilizing stimulus representations in primate prefrontal cortical activity. *Cell Reports* **36**, 109469 (2021).
30. Tang, Y. & Aigner, T. G. Release of cerebral acetylcholine increases during visually mediated behavior in monkeys. *Neuroreport* **7**, 2231–2235 (1996).
31. Münch, M. et al. Different colors of light lead to different adaptation and activation as determined by high-density EEG. *Neuroimage* **101**, 547–554 (2014).
32. Rokszin, A. A. et al. The interplay of holistic shape, local feature and color information in object categorization. *Biol. Psychol.* **109**, 120–131 (2015).
33. Wang, L. et al. Color design for illustrative visualization. *IEEE Trans. Vis. Comput. Graph.* **14**, 1739–1754 (2008).
34. Wang, W. et al. Strain-insensitive intrinsically stretchable transistors and circuits. *Nature Electronics* **4**, 143–150 (2021).
35. Dai, Y. et al. Stretchable redox-active semiconducting polymers for high-performance organic electrochemical transistors. *Advanced Materials* **34**, 2201178 (2022).
36. Lu, T. & Chen, F. Multiwfn: A Multifunctional Wavefunction Analyzer. *J. Comput. Chem.* **33**, 580–592 (2012).

Acknowledgements

This work was supported by the Strategic Priority Research Program of CAS (XDB0520101), the National Natural Science Foundation of China (U22A6002, T2441002, 52403395, and 51925306), the CAS Project for Young Scientists in Basic Research (YSBR-053), the National Key R&D Program of China (2022YFB3603804 and 2021YFB3200701), and the China Postdoctoral Science Foundation (2025T180031, 2023M743440 and GZC20232599), the Advanced In-situ Characterization Facility of Molecular Condensed and Electronic Structures (AIC-MCES).

Author contributions

Y.L., H.H. and Y.G. conceived the idea. G.L. carried out most of the experiments and data analysis. W.W. performed the film spectral characterization. C.S. performed the neural network simulation. Ha.H. carried out the theoretical calculations. Y.Z. helped the TOF-SIMS test. Y.B. helped the device fabrication. G.L. and Y.G. wrote and revised the manuscript. Y.L., H.H. and Y.G. guided the whole project. All authors discussed the progress of the research and reviewed the paper.

Competing interests

The authors declare no competing interests.

Additional information

Supplementary information The online version contains supplementary material available at https://doi.org/10.1038/s41467-025-61783-1.

Correspondence and requests for materials should be addressed to Yunlong Guo, Hui Huang or Yunqi Liu.

Peer review information *Nature Communications* thanks the anonymous reviewers for their contribution to the peer review of this work. A peer review file is available.